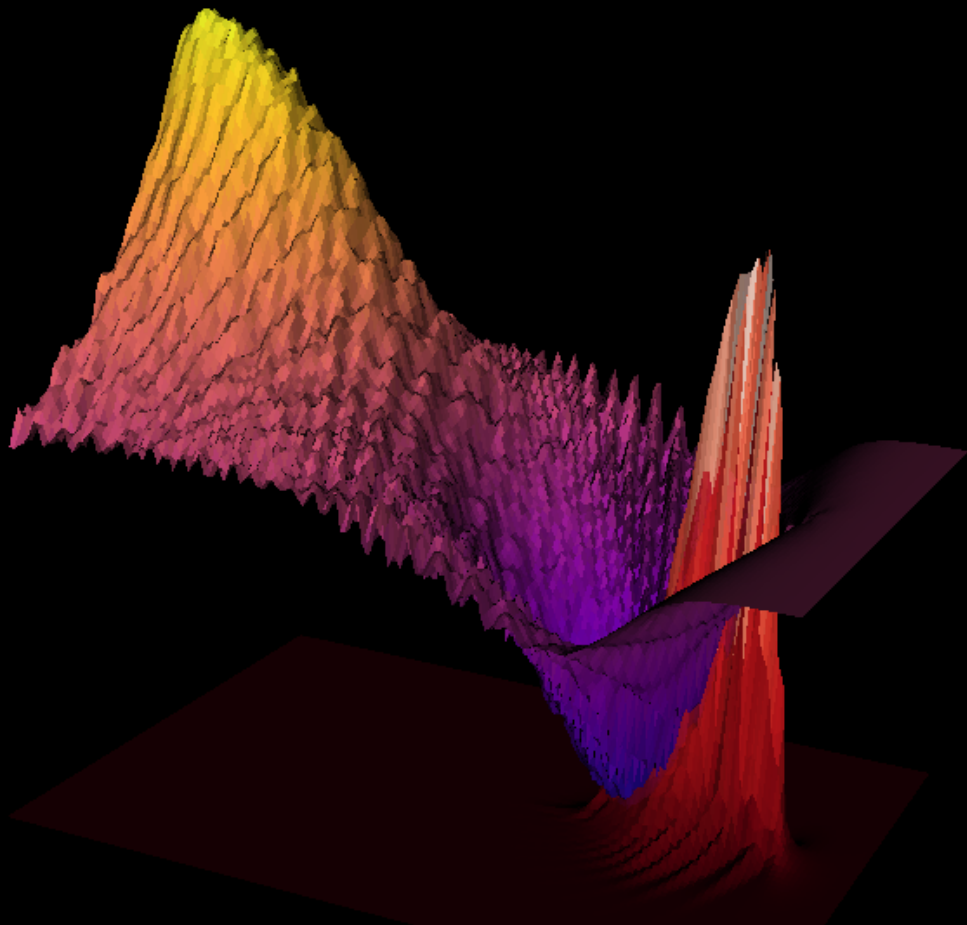


MASTER'S THESIS 2019

# A compact plasma beam dump for next generation particle accelerators

OSCAR JAKOBSSON



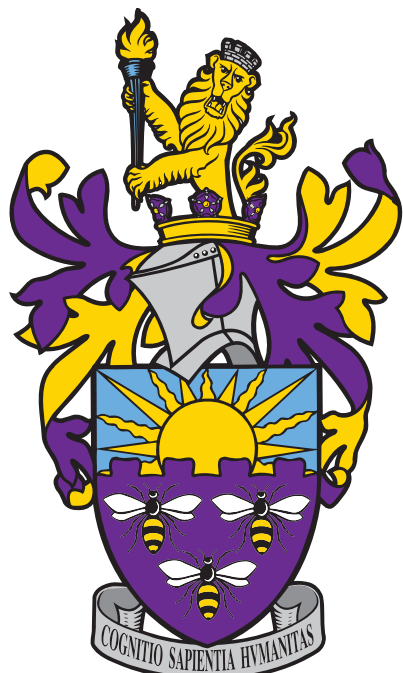
SCHOOL OF PHYSICS AND ASTRONOMY  
THE UNIVERSITY OF MANCHESTER





# A compact plasma beam dump for next generation particle accelerators

OSCAR JAKOBSSON



School of Physics and Astronomy  
*Cockcroft Accelerator Group*  
THE UNIVERSITY OF MANCHESTER  
Manchester, United Kingdom 2019

A compact plasma beam dump for next generation particle accelerators  
OSCAR JAKOBSSON

© OSCAR JAKOBSSON, 2017.

Supervisor: Guoxing Xia, Cockcroft Accelerator Group

Master's Thesis 2019  
School of Physics and Astronomy  
Cockcroft Accelerator Group  
The University of Manchester

Cover: Wind visualization constructed in Matlab showing a surface of constant wind speed along with streamlines of the flow.

Typeset in L<sup>A</sup>T<sub>E</sub>X

A compact plasma beam dump for next generation particle accelerators

OSCAR JAKOBSSON

School of Physics and Astronomy

The University of Manchester

## Abstract

Lore ipsum dolor sit amet, consectetur adipisicing elit, sed do eiusmod tempor incididunt ut labore et dolore magna aliqua. Ut enim ad minim veniam, quis nostrud exercitation ullamco laboris nisi ut aliquip ex ea commodo consequat. Duis aute irure dolor in reprehenderit in voluptate velit esse cillum dolore eu fugiat nulla pariatur. Excepteur sint occaecat cupidatat non proident, sunt in culpa qui officia deserunt mollit anim id est laborum.

Keywords: Plasma wakefield acceleration, deceleration, beam dump, ILC, EuPRAXIA



## Acknowledgements

  Lorem ipsum dolor sit amet, consectetur adipisicing elit, sed do eiusmod tempor incididunt ut labore et dolore magna aliqua. Ut enim ad minim veniam, quis nostrud exercitation ullamco laboris nisi ut aliquip ex ea commodo consequat. Duis aute irure dolor in reprehenderit in voluptate velit esse cillum dolore eu fugiat nulla pariatur. Excepteur sint occaecat cupidatat non proident, sunt in culpa qui officia deserunt mollit anim id est laborum.

Oscar Jakobsson, Manchester, January 2019



# Contents

<b>List of Figures</b>	<b>xi</b>
<b>1 Introduction</b>	<b>1</b>
1.1 Conventional accelerators . . . . .	1
1.2 Plasma wakefield accelerators . . . . .	1
1.3 EuPRAXIA . . . . .	1
1.4 Thesis Outline . . . . .	1
<b>2 Theory</b>	<b>3</b>
2.1 PWFA - Linear-Fluid Wakefield Theory . . . . .	3
2.1.1 Plasma Dynamics - fluid model . . . . .	3
2.1.2 Density perturbations . . . . .	3
2.1.3 Longitudinal Accelerating Field . . . . .	4
2.1.4 Transverse Focusing Field . . . . .	7
2.2 Non-linear Regime . . . . .	8
2.2.1 Wave-breaking field . . . . .	8
2.3 Particle interactions with matter . . . . .	11
2.3.1 Bohr-Fermi-Bethe-Bloch Theory . . . . .	11
2.3.2 Collective Plasma Deceleration – Non-Linear regime . . . . .	11
2.3.3 Collective Plasma Deceleration – Linear regime . . . . .	12
2.3.4 Notes Bonatto . . . . .	14
<b>3 Simulations</b>	<b>15</b>
3.1 Plasma simulations . . . . .	15
3.2 Particle-in-Cell Codes . . . . .	16
3.3 EPOCH . . . . .	17
3.3.1 Input deck and initial conditions . . . . .	17
3.3.2 Grid settings . . . . .	17
3.3.3 Non-analytical bunch initialisation . . . . .	18
3.4 Notes. . . . .	19
<b>4 Simulation tests</b>	<b>21</b>
4.1 Plasma deceleration - Uniform density . . . . .	21
4.1.1 Transverse instabilities in quasilinear regime . . . . .	21
4.2 Hybrid Scheme - Feasibility study . . . . .	21
4.2.1 Initialising a decelerated bunch . . . . .	21
4.2.2 Introduction of co-propagating laser . . . . .	21

## Contents

---

5 Ongoing and future work	23
6 Conclusion	25
Bibliography	27
A Appendix: Input decks	I

# List of Figures

2.1	Plot corresponding to Dawson's derivation of the wave-breaking field [ref. Sahai].	10
2.2	Non-linear regime, plasma density perturbations. Added custom legend with density=number of electrons / grid-square size.	12
2.3	Should these three plots be in results or here? OR PUT SIMUALTIONS CHAPTER BEFORE THEORY CHAPTER. Then theory can be used to also verify that simulations work. Probably not, better explain everything to motivate what simulations to be done	13

## List of Figures

---

# 1

## Introduction

### 1.1 Conventional accelerators

Conventional accelerators, RF cavities and limited acceleration , beam dump for small to future accelerators, difficulties of beam dumping only getting worse with increasing energy.

### 1.2 Plasma wakefield accelerators

Plasma wakefield accelerators as an alternative to accelerators. History (Tajima/Dawson), how it works, progress/challenges. Recent research also shows that L/PWFA may be a good substitute for the deceleration of the beam as well, regardless of whether the beam is accelerated in wake fields or RF cavities. Describe previous work Tajima's paper (passive), Hanahoe (varying density), Bonatto (active). In this thesis we explore these schemes, and attempt to merge the active and varying density approach in what we call a hybrid scheme. All simulations are carried out with a 1GeV 30pc so-called EuPRAXIA electron beam.

### 1.3 EuPRAXIA

EuPRAXIA (European Plasma Research Accelerator with eXcellence In Applications)

### 1.4 Thesis Outline

This intermediate report details the initial phase of a full-year project on plasma wakefield deceleration and is written in partial fulfilment of the requirements for the degree of Master in Physics. As such, it does not attempt to cover the full scope of the work and research conducted in the first half of this project, but rather aims to provide and introduction to the field, establish the theoretical background and construct the computational framework necessary to perform the research we desire. Having lain the groundwork for the project in this report, the the final-year report will reap the rewards of this work by presenting the full results and outcome of the project.

The theory behind plasma wakefield acceleration and plasma beam dumps is covered in section 2. The simulation framework is detailed in section 3, followed by simulation tests and preliminary results in section 4. We conclude this report by summarising the work that has been presented and looking ahead at the work that is to be carried out in the second half of

## 1. Introduction

this project. Sections:

- Theory (PWFA, LWFA, energy loss etc.)
- Simulation (PIC, EPOCH description, set up framework (“building the experiment”))
- Preliminary results (low res results) (wide bunch, varying plasma density, hybrid scheme)(Nothing conclusive just results to show that the simulations have been set up correctly)
- Conclusion + looking ahead

# 2

## Theory

### 2.1 PWFA - Linear-Fluid Wakefield Theory

#### 2.1.1 Plasma Dynamics - fluid model

What is the wave-breaking field  $E_Z$ , why is it the maximum possible acceleration/deceleration field? Is it always reached?

$$\omega_p = \sqrt{\frac{4\pi e^2 n_0}{m_e}} \quad (2.1)$$

#### 2.1.2 Density perturbations

Continuity equation

$$\frac{\partial n}{\partial t} = -\nabla \cdot (n\mathbf{v}) \quad (2.2)$$

where  $n$  is the plasma density and  $\mathbf{v}$  the plasma fluid velocity. Charge conservation.  
Lorentz force law:

$$m_e \frac{\partial n\mathbf{v}}{\partial t} = en \left( \mathbf{E} + \frac{\mathbf{v} \times \mathbf{B}}{c} \right) \quad (2.3)$$

Treating the plasma response to a particle beam perturbatively we have  $n(r, z, t) = n_0 + n_1(r, z, t)$  where  $n_0$  is the ion density and  $n_1$  the plasma perturbation. We let  $\mathbf{v}, \mathbf{E}, \mathbf{B}$  be perturbative responses to the beam. From continuity equation we have

$$\frac{\partial n_0}{\partial t} + \frac{\partial n_1}{\partial t} = -\nabla \cdot (n_0\mathbf{v}) - \nabla \cdot (n_1\mathbf{v}) \quad \Rightarrow \quad \frac{\partial n_1}{\partial t} \approx -n_0 \nabla \cdot (\mathbf{v}) \quad (2.4)$$

From the Lorentz force law have

$$m_e n_0 \frac{\partial(1 + n_1/n_0)\mathbf{v}}{\partial t} \approx en_0(1 + n_1/n_0)\mathbf{E} \quad \Rightarrow \quad m_e \frac{\partial \mathbf{v}}{\partial t} \approx e\mathbf{E} \quad (2.5)$$

which, using Gauss's law, gives

$$\frac{\partial(\nabla \cdot \mathbf{v})}{\partial t} \approx \frac{e}{m_e} \nabla \cdot \mathbf{E} = \frac{e^2}{m_e} 4\pi(n_1 + n_b) \quad (2.6)$$

where  $n_1 + n_b$  is the free charge. Hence

$$\frac{\partial^2 n_1}{\partial t^2} = -n_0 \frac{\partial(\nabla \cdot \mathbf{v})}{\partial t} = -\frac{4\pi n_0 e^2}{m_e} (n_1 + n_b) \quad (2.7)$$

which gives

$$\frac{\partial^2 n_1}{\partial t^2} + \omega_p^2 n_1 = -\omega_p^2 n_b \quad (2.8)$$

where the  $\omega_p = (4\pi e^2 n_0 / m_e)^{1/2}$  is the plasma frequency. We can rewrite this expression in the reference frame of the beam.

Perturbation due to beam  $n(r, \xi) \rightarrow n(r, \xi) + n_1(r, \xi)$ , use Maxwell's equations and continuity equation.

$$-\frac{1}{k_p^2} \left( \frac{\partial^2}{\partial \xi^2} + k_p^2 \right) n_1(r, \xi) = n_b(r, \xi) , \quad n_1(r, \xi < 0) = 0 \quad (2.9)$$

$$\mathcal{L}_\xi n_1(r, \xi) = n_b(r, \xi) \Rightarrow \mathcal{L}_\xi G(\xi, \xi') = \delta(\xi - \xi') \quad (2.10)$$

$$G(\xi, \xi') = \begin{cases} 0 & , -\infty < \xi < \xi' \\ A \sin(k_p \xi) + B \cos(k_p \xi) & , \xi' < \xi < \infty \end{cases} \quad (2.11)$$

where the Green's function obeys the same b.c as the density perturbation, i.e it is continuous across the boundary with a discontinuous derivative across the boundary. Integrate across discontinuity at  $\xi = 0$

$$\lim_{\epsilon \rightarrow 0} \int_{\xi' - \epsilon}^{\xi' + \epsilon} \mathcal{L}_\xi G(\xi, \xi') d\xi = \lim_{\epsilon \rightarrow 0} \int_{\xi' - \epsilon}^{\xi' + \epsilon} \delta(\xi) d\xi = 1 \Rightarrow \lim_{\epsilon \rightarrow 0} \left[ -\frac{1}{k_p^2} \frac{\partial G}{\partial \xi} \right]_{\xi' - \epsilon}^{\xi' + \epsilon} = 1 \quad (2.12)$$

Without loss of generality we may set the arrival of the beam to be at  $t = 0$ , such that  $\xi' = 0$ .

$$G(\xi, \xi') = -k_p \sin(k_p \xi) \Theta(\xi) \Rightarrow n_1(r, \xi) = \int_{-\infty}^{\infty} G(\xi, \xi') n_b(r, \xi') d\xi' \quad (2.13)$$

### 2.1.3 Longitudinal Accelerating Field

$$\nabla \times \mathbf{E} = -\frac{1}{c} \frac{\partial \mathbf{B}}{\partial t} \quad (2.14)$$

$$\nabla \times \mathbf{B} = \frac{4\pi}{c} \mathbf{J} + \frac{1}{c} \frac{\partial \mathbf{B}}{\partial t} \quad (2.15)$$

gives

$$\nabla^2 \mathbf{E} - \frac{1}{c^2} \frac{\partial^2 \mathbf{E}}{\partial t^2} = \frac{4\pi}{c^2} \frac{\partial \mathbf{J}}{\partial t} + 4\pi \nabla \rho \quad (2.16)$$

Lorentz force law ( $\mathbf{v}$  is the velocity of the plasma):

$$m \frac{\partial n \mathbf{v}}{\partial t} = en \left( \mathbf{E} + \frac{\mathbf{v} \times \mathbf{B}}{c} \right) \approx en \mathbf{E} \Rightarrow \frac{\partial \mathbf{J}_p}{\partial t} = \frac{e^2 n}{m} \mathbf{E} \quad (2.17)$$

Letting  $\rho = \rho_b + \rho_p$  and  $\mathbf{J} = \mathbf{J}_b + \mathbf{J}_p$  for the beam and plasma respectively, and  $\mathbf{J}_b = c \rho_b \hat{\mathbf{z}}$ , gives

$$\left( \nabla^2 - \frac{1}{c^2} \frac{\partial^2}{\partial t^2} - k_p^2 \right) \mathbf{E} = \frac{4\pi}{c} \frac{\partial \rho_b}{\partial t} \hat{\mathbf{z}} + 4\pi \nabla (\rho_b + \rho_p) \quad (2.18)$$

where  $k_p = \omega_p/c$  is the plasma wave number. To find the electric field along the beam, z-direction, we proceed by solving

$$\left( \nabla^2 - \frac{1}{c^2} \frac{\partial^2}{\partial t^2} - k_p^2 \right) E_z = \frac{4\pi}{c} \frac{\partial \rho_b}{\partial t} + 4\pi \frac{\partial}{\partial z} (\rho_b + \rho_p) \quad (2.19)$$

using  $\nabla^2 = \nabla_{\perp}^2 + \frac{\partial^2}{\partial z^2}$ , in Fourier transform space, where

change this to  $E=\text{integral tilde } E$ , then substitute that into the following equations, since the RHS of 2.14 is not correct, fourier transform of the derivative acting on the function is not the same as the derivative acting on the transformed function

$$E_z(\xi)(k) = \int_{-\infty}^{\infty} \tilde{E}_z(k) e^{ik\xi} dk , \quad (\rho_b(k) + \rho_p(k)) = \int_{-\infty}^{\infty} (\tilde{\rho}_b(\xi) + \tilde{\rho}_p)(\xi) e^{ik\xi} d\xi \quad (2.20)$$

such that

$$\left( \frac{\partial^2}{\partial z^2} - \frac{1}{c^2} \frac{\partial^2}{\partial t^2} \right) E_z(\xi) = 0 \quad (2.21)$$

and

$$\frac{4\pi}{c} \frac{\partial \rho_b}{\partial t} + 4\pi \frac{\partial}{\partial z} (\rho_b + \rho_p) = -4\pi i k \tilde{\rho}_b + 4ik\pi \tilde{\rho}_b + 4ik\pi \tilde{\rho}_p = 4ik\pi \tilde{\rho}_p \quad (2.22)$$

which gives

$$\left( \nabla_{\perp}^2 - k_p^2 \right) \tilde{E}_z(\xi) = 4\pi i k \tilde{\rho}_p \quad (2.23)$$

We note that the two contributions from the beam cancel each other out, this is because of relativistic effects (?) [? ]. From eq. XXX we have

$$\frac{\partial^2 \rho_p}{\partial t^2} + \omega_p^2 \rho_p = -\omega_p^2 \rho_b \Rightarrow -k^2 \tilde{\rho}_p + k_p^2 \tilde{\rho}_p = -k_p^2 \tilde{\rho}_b \Rightarrow \tilde{\rho}_p = \frac{k_p^2}{k^2 - k_p^2} \tilde{\rho}_b \quad (2.24)$$

$$\nabla_{\perp}^2 = \frac{1}{r} \frac{\partial}{\partial r} r \frac{\partial}{\partial r} + \frac{1}{r^2} \frac{\partial^2}{\partial \phi^2} \quad (2.25)$$

$$\left( \frac{\partial^2}{\partial r^2} + \frac{1}{r} \frac{\partial}{\partial r} - k_p^2 \right) \tilde{E}_z = 4\pi i k_p^2 \frac{k}{k^2 - k_p^2} \tilde{\rho}_b \quad (2.26)$$

We now rewrite this equation as

$$\mathcal{L} \tilde{E}_z = \tilde{f}(r) \quad (2.27)$$

We proceed as before and solve this PDE by finding the Green's function. Working in a cylindrical coordinate system we have that the Green's function must satisfy

$$\mathcal{L} G(\mathbf{r}, \mathbf{r}') = \delta(\mathbf{r} - \mathbf{r}') = \frac{1}{r} \delta(r - r') \delta(\phi - \phi') \delta(z - z') \quad (2.28)$$

where the RHS is the 3D Dirac delta function in cylindrical polar coordinates, defined such that  $\int \delta(\mathbf{r} - \mathbf{r}') r dr d\phi dz = 1$ . Letting

$$G(\mathbf{r}, \mathbf{r}') = G_r(r, r') \delta(\phi - \phi') \delta(z - z') \quad (2.29)$$

leads to

$$\mathcal{L} G_r(r, r') = \frac{1}{r} \delta(r - r') \quad (2.30)$$

## 2. Theory

---

The LHS of this expression is the modified Bessel function of order zero and the RHS represents our source term. Consequently the Green's function is formed by linear combinations of, the linearly independent, modified Bessels functions of order zero.

$$G(r, r') = \begin{cases} A(r')(A_1 I_0(k_p r) + B_1 K_0(k_p r)) & , 0 < r < r' \\ B(r')(A_2 I_0(k_p r) + B_2 K_0(k_p r)) & , r' < r < \infty \end{cases} \quad (2.31)$$

requiring that the two parts of this expression each satisfy one of the B.Cs we have that  $B_1 = A_2 = 0$  since  $K_0(k_p r) \rightarrow \infty$  as  $r \rightarrow 0$  and  $I_0(k_p r) \rightarrow \infty$  as  $r \rightarrow \infty$ . Continuity in  $G(r, r')$  at  $r = r'$  further gives that

$$G(r, r') = A_0 \begin{cases} I_0(k_p r)K_0(k_p r') & , 0 < r < r' \\ I_0(k_p r')K_0(k_p r) & , r' < r < \infty \end{cases} \quad (2.32)$$

where  $A_0$  is a constant of proportionality that we find by integrating  $\mathcal{L}G(r, r') = \delta(r - r')/r$  with respect to  $r$  across the interval  $[r' - \epsilon, r' + \epsilon]$ , which needs to be satisfied for all  $\epsilon$ , including the limit as  $\epsilon \rightarrow 0$ .

$$\lim_{\epsilon \rightarrow 0} \int_{r'-\epsilon}^{r'+\epsilon} \left( \frac{\partial^2 G}{\partial r^2} + \frac{1}{r} \frac{\partial G}{\partial r} - k_p^2 G \right) dr = \lim_{\epsilon \rightarrow 0} \int_{r'-\epsilon}^{r'+\epsilon} \frac{1}{r} \delta(r - r') dr = \frac{1}{r'} \quad (2.33)$$

$$\lim_{\epsilon \rightarrow 0} \left[ \frac{1}{k_p} \frac{\partial G}{\partial r} \right]_{z-\epsilon}^{z+\epsilon} = \frac{A_0}{k_p} \left( I_0(k_p r') \frac{\partial K_0(k_p r)}{\partial r} - \frac{\partial I_0(k_p r)}{\partial r} K_0(k_p r') \right) \Big|_{r=r'} = \frac{1}{r'} \quad (2.34)$$

This equality must hold for all values of  $r'$ . Hence, following an approach by Jackson [1], we evaluate the LHS for  $r' \gg 1$ , where  $I_0$  and  $K_0$  take the limiting forms

$$I_0(k_p r') \rightarrow \frac{1}{\sqrt{2\pi k_p r'}} e^{k_p r'} \quad \text{and} \quad K_0(k_p r') \rightarrow \sqrt{\frac{\pi}{2k_p r'}} e^{-k_p r'} \quad (2.35)$$

which implies that  $A_0 = -1$ . Here Gessner gets  $A = 4\pi$  because of Jackson but I don't see why.

$$G(r, r') = -I_0(k_p r)K_0(k_p r')\Theta(r' - r) - I_0(k_p r')K_0(k_p r)\Theta(r - r') \quad (2.36)$$

We can thus find  $\tilde{E}_z$  from

$$\tilde{E}_z(r, k) = \int_{-\infty}^{\infty} G(r, r') f(r', k) r' dr' \quad (2.37)$$

and then perform an inverse Fourier transform to find

$$E_z(r, \xi) = \frac{1}{2\pi} \int_{-\infty}^{\infty} \tilde{E}_z(r, k) e^{ik\xi} dk \quad (2.38)$$

Doing this yields

$$E_z(r, \xi) = \frac{4\pi i k_p^2}{2\pi} \int_{-\infty}^{\infty} \frac{ke^{ik\xi}}{k^2 - k_p^2} dk \int_0^{\infty} G(r, r') \tilde{\rho}_b(r') r' dr' \quad (2.39)$$

$$= -2\pi k_p^2 \cos(k_p \xi) \Theta(\xi) \int_0^{\infty} G(r, r') \tilde{\rho}_b(r') r' dr' \quad (2.40)$$

Where the  $\Theta(\xi)$  has been added due to causality.

Now lets solve this for a bi-Gaussian beam charge distribution. To do this, we may compute the electric field from the Green's function directly and then carrying out the inverse Fourier transform, or we could choose to first compute the field due to a point-particle and then convolving it with the bi-Gaussian distribution. We proceed by doing the latter by choosing a charge distribution with radial symmetry and a delta function in the  $z$ -direction to match our Green's function.

$$\rho_{b_0}(r, \xi) = \frac{e}{2\pi r} \delta(r - r_0) \delta(\xi) \Rightarrow \tilde{\rho}_{b_0}(r, k) = \int_{-\infty}^{\infty} \rho_b(r, \xi) e^{-ik\xi} d\xi = \frac{e}{2\pi r} \delta(r - r_0) \quad (2.41)$$

which gives

$$\tilde{E}_z(r, k) = -2ek_p^2 \frac{k}{k^2 - k_p^2} G(r, r_0) \quad (2.42)$$

which satisfies (2.26), as can be shown by integrating across the discontinuity and taking the limit to zero, and then gives

$$E_z(r, \xi) = -ek_p^2 \cos(k_p \xi) G(r, r_0) \Theta(\xi) \quad (2.43)$$

**But my Green's function has a  $A = -1$  as constant and not  $A = 4\pi$  as Bonatto and Gessner**  
 This is refer to as the single-particle wake function [? ]. The longitudinal electric field resulting from an arbitrary source distribution  $n_b(r, \xi)$  is given by the convolution of the source by the single-particle wake function:

$$E_z(r, \xi) = -ek_p^2 \int_{-\infty}^{\infty} \cos(k_p(\xi - \xi')) \Theta(\xi - \xi') d\xi' \int_0^{\infty} G(r, r_0) n_b(r_0, \xi') r' dr' \quad (2.44)$$

$$= -ek_p^2 \int_{-\infty}^{\xi} \cos(k_p(\xi - \xi')) d\xi' \int_0^{\infty} G(r, r_0) n_b(r_0, \xi') r_0 dr_0 \quad (2.45)$$

which is not the same as Bonatto/Gessner/Schroeder, the limits are different, they have from xi to infinity , is this not how to do a convolution? Why don't we have something like  $r - r'$  from a radial convolution or something? Bonatto, Schroder has the integral from infinity to xi, why?

These expressions with  $-4\pi$  does not satisfy the diff.eq that I am trying to solve in transform space, so why do they use them if they don't solve their original diff. equations?

Mira's thesis also has  $4\pi$  if converting to cgs.

### 2.1.4 Transverse Focusing Field

Use Panofsky-Wenzel theorem

## 2.2 Non-linear Regime

### 2.2.1 Wave-breaking field

Dawson's derivation [Note: The wave-breaking field does not represent the onset of the non-linear regime but the highest achievable field in the non-linear regime.] We consider a simple 1D linear non-relativistic electron sheet model first used by Dawson [2] to show the breakdown of the linear model (**correct?**). Consider the plasma being made up of thin sheets of ions and electrons. A sheet at equilibrium position  $z = z_0$  is then displaced by  $\eta_0(z_0)$ , where the displacement is set as function of the equilibrium position for full generality, to a new position  $z = z_0 + \eta_0$ . The displaced sheet reveals a positive surface charge density  $\sigma = en_0\eta_0$ , where  $n_0$  is the electron charge density in the plasma. This sets up a restoring electric field which we find using Gauss's law to be  $E_{\text{res}} = 4\pi n_0 e \eta_0$  which yields a restoring force

$$m_e \frac{\partial^2 \eta_0}{\partial t^2} = -eE_{\text{res}} = -4\pi n_0 e^2 \eta_0 = -\omega_p^2 \eta_0 \quad (2.46)$$

with solutions

$$\eta_0(z_0, t) = A_1(z_0) \cos(\omega_p t) + A_2(z_0) \sin(\omega_p t) \quad (2.47)$$

The phenomena of wave breaking can be shown by considering another electron sheet at an equilibrium position  $z_1 = z_0 + \Delta z_0$  at a distance  $\Delta z_0$  away from the first sheet. This sheet is then displaced by  $\eta_1$  to a new position  $z_1^* = z_0 + \Delta z_0 + \eta_1$ . The linear model is valid provided that there are no electron trajectories intersect one another in the plasma [**is this correct? Why does the model break down?** ]. Hence the model is valid provided that  $z_1^* - z_0 > z - z_0$  which implies that we must have

$$\Delta z_0 + \eta_1 > \eta_0 , \quad (2.48)$$

for all  $\Delta z_0 \in \mathbb{R}$ , to sustain plasma oscillations in the linear model. We now consider the limit as  $\Delta z_0 \rightarrow 0$  for the expression

$$\frac{\partial \eta}{\partial x_0} = \lim_{\Delta z_0 \rightarrow 0} \frac{\Delta \eta}{\Delta z_0} = \lim_{\Delta z_0 \rightarrow 0} \left( \frac{\eta_1 - \eta_0}{\Delta z_0} \right) > \lim_{\Delta z_0 \rightarrow 0} \left( \frac{\eta_0 - \Delta z_0 - \eta_0}{\Delta z_0} \right) = -1 \quad (2.49)$$

which simplifies to

$$\frac{\partial \eta}{\partial z_0} > -1 \quad (2.50)$$

where the inequality is introduced using Eq. (2.48). We now consider the special case where  $A_1(z_0) = A \sin(k_p z_0)$  and  $A_2(z_0) = 0$ . This is a valid solution since  $\sin(k_p z_0)$  is single-valued for all  $k_p, x_0 \in \mathbb{R}$ . This particular solution is chosen to highlight the breakdown of the electric field, and is motivated by ([what?]) the solution we found for the electric field in section 2. Applying the no-crossing criterion in Eq. 2.50 to  $\eta = \eta_0(z_0, t)$  yields

$$\frac{\partial \eta_0}{\partial z_0} = Ak_p \cos(k_p z_0) > -1 \Leftrightarrow Ak_p \leq 1 \quad (2.51)$$

which gives the maximum amplitude as  $A_{\max} = 1/k_p$ . Hence the maximum restoring electric field  $E_{\max} \equiv E_{\text{wb}} = 4\pi n_0 / k_p$  is given by

$$E_{\text{wb}} = \frac{m_e v_p \omega_p}{e} \quad (2.52)$$

the so-called *wave-breaking field*. To further show how this breaks the linear model we consider the effect on the electric field up to and past the wave-breaking limit. As above we have,

$$z = z_0 + \eta_0 = z_0 + A \sin(k_p z_0) \quad (2.53)$$

and

$$E = 4\pi n_0 e A \sin(k_p z_0) \quad (2.54)$$

from which we want to find the electric field as a function of  $z$ . We can do this by numerically solving Eq. 2.53 for  $z_0$  in a range of  $z$  values given fixed values of  $A$ . This gives  $z_0 = z_0(z, A)$  which can be substituted into Eq. 2.54 to give  $E = E(z, A)$ , the result of which is shown in Fig. 2.1. From this we conclude that the electric field is no longer single-valued for  $A > 1/k_p$ , i.e past the electric field's wave-breaking amplitude, which signifies a breakdown of the linear model.

This is further emphasized by consider the electron-density response as  $\partial\eta/\partial z_0 \rightarrow -1$ . To do this we use Eq. XXX in 1D with no beam density  $n_b = 0$ ,

$$\frac{\partial E}{\partial z} = 4\pi e(n_0 - n) \quad (2.55)$$

where  $n = n_0 + n_1$  is the perturbed plasma density and  $n_0$  is the ion density, hence  $n_0 - n$  is the free (negative) charge density in the plasma. We now take the derivative of the perturbed electric field and substitute the above expression

$$\frac{\partial E}{\partial z} = 4\pi n_0 e \frac{\partial \eta}{\partial z} \Rightarrow n = n_0 \left(1 - \frac{\partial \eta}{\partial z}\right) \quad (2.56)$$

We now rewrite  $\partial/\partial z$ , using  $z = z_0 + \eta$ , as

$$\frac{\partial}{\partial z} = \left(1 - \frac{\partial \eta}{\partial z_0}\right)^{-1} \frac{\partial}{\partial z_0} \quad (2.57)$$

which gives

$$n = \frac{n_0}{1 + \frac{\partial \eta}{\partial z_0}} \quad (2.58)$$

which means that the perturbed electron density grows infinite as  $\partial\eta/\partial z_0 \rightarrow -1$ , again signifying the breakdown of the linear model.

Having seen that the linear theory can break down mathematically, it is crucial to ask whether this is realised in 3D models and experiments as well.

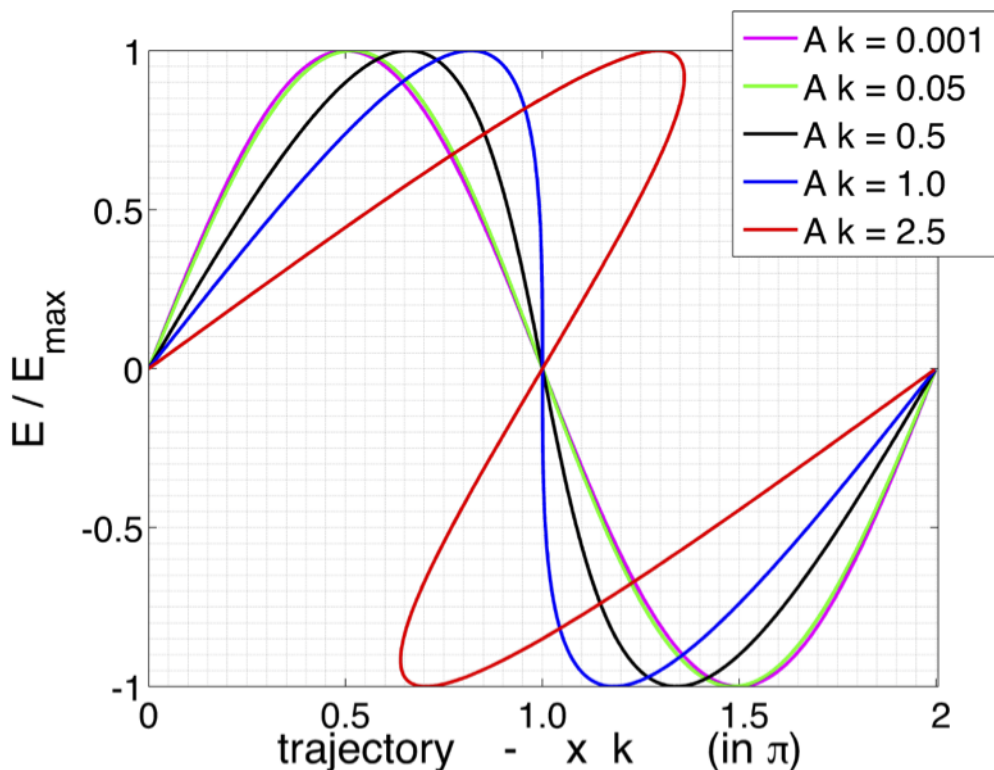


**Figure 2.1:** Plot corresponding to Dawson's derivation of the wave-breaking field [ref. Sahai].

## 2.3 Particle interactions with matter

Conventional beam dumps work by stochastic interactions of the beam with the dense medium [hanahoe 6.5]

### 2.3.1 Bohr-Fermi-Bethe-Bloch Theory

Bethe-Bloch formula:

$$-\left\langle \frac{dU}{ds} \right\rangle_{\text{ion}} = \frac{4\pi e^4 n_{e,m}}{m_e c^2 \beta^2} \left[ \ln \left( \frac{2m_e \gamma^2 v^2}{I} \right) - \beta^2 \right] \quad (2.59)$$

### 2.3.2 Collective Plasma Deceleration – Non-Linear regime

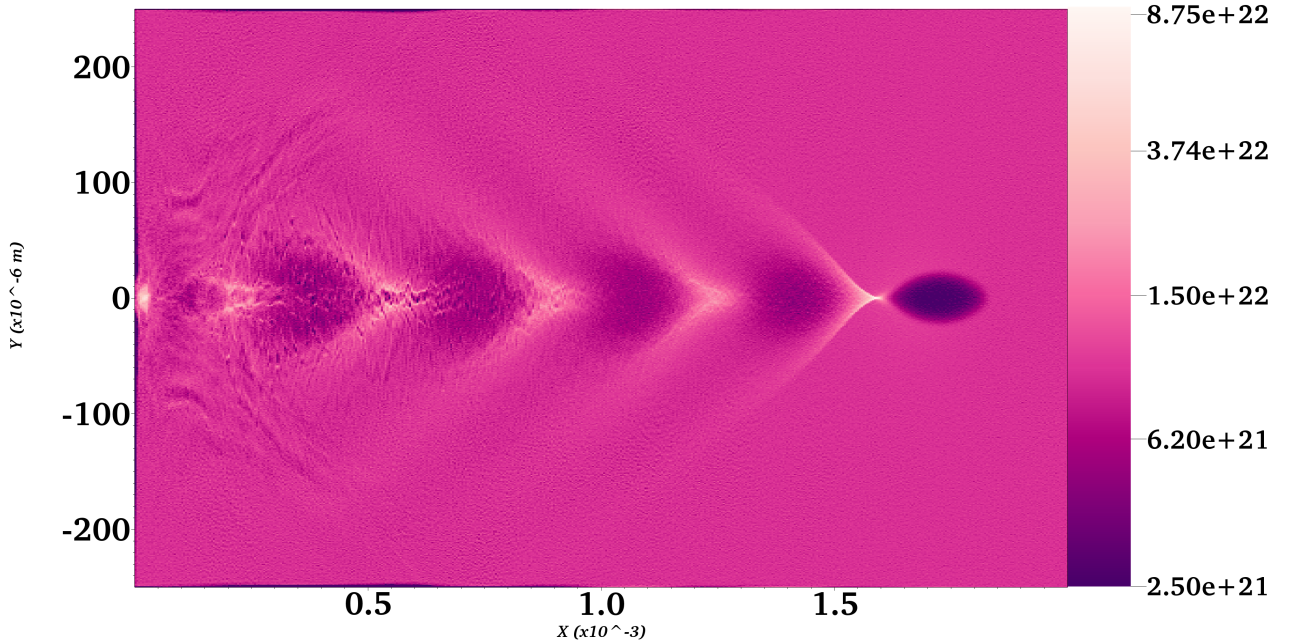


**Figure 2.2:** Non-linear regime, plasma density perturbations. Added custom legend with density=number of electrons / grid-square size.

$$-\left(\frac{dE}{dz}\right)_{\text{coll-wave-break}} = F_e = eE_{\text{wave-break}} = m_e c \omega_p \left(\frac{n_b}{n_e}\right) \quad (2.60)$$

What is the wave-breaking electric field?

### 2.3.3 Collective Plasma Deceleration – Linear regime

Based on the work of Lu et. al [3], wherein it was shown that the predictions from the linear models perform well even in the non-linear regime, it is of interest to compute the energy loss in the linear regime. This follows the analysis by Bonatto et al. [4].

The energy loss of a bunch is due to the work carried out by the longitudinal electric field  $E_z$ , neglecting effects such as bremsstrahlung etc. The rate of energy change with propagation distance of a particle at position  $(r, \xi)$  in the bunch after travelling is given by the force exerted on the particle by the longitudinal electric field:

$$\frac{dU_p}{ds} = -eE_z(r, \xi) \quad (2.61)$$

where we have assumed that there occurs no modulation of the particle bunch as it traverses the plasma, hence the electric field is only a function of the position in the bunch  $E_z(r, \xi)$  and not the propagation distance  $s$ . Integrating over the propagation distance then gives

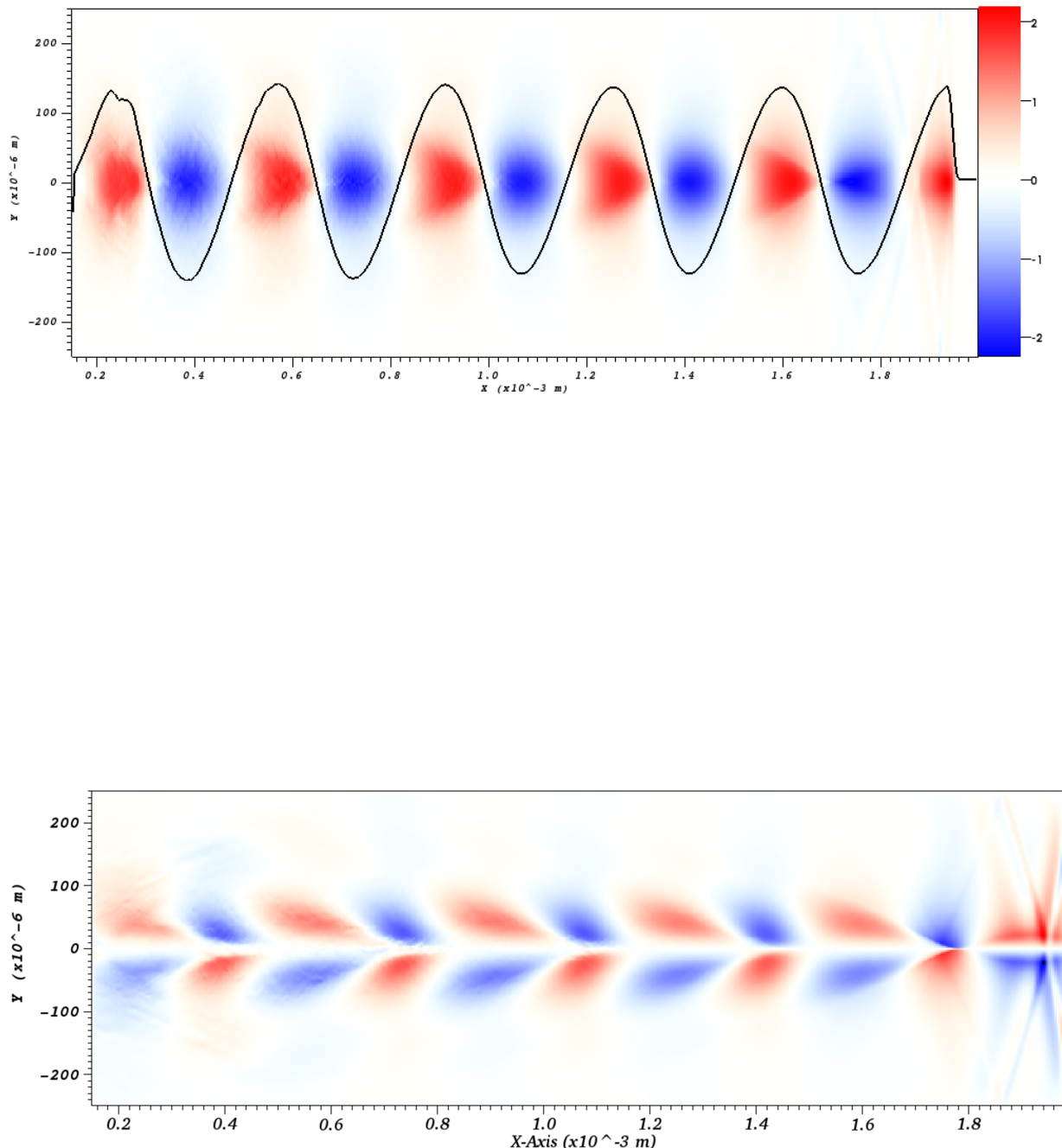


**Figure 2.3:** Should these three plots be in results or here? OR PUT SIMUALTIONS CHAPTER BEFORE THEORY CHAPTER. Then theory can be used to also verify that simulations work. Probably not, better explain everything to motivate what simulations to be done

the energy of one particle in the beam at position  $(r, \xi)$  after travelling a distance  $s$ :

$$U_e(r, \xi, s) = U_e(r, \xi, 0) - seE_z(r, \xi) \quad (2.62)$$

from which multiplication by the beam number density  $n_b(r, \xi)$  and integration over the volume of the bunch gives the total energy of all particles in the bunch after propagation distance  $s$

$$U(s) = \int U_e(r, \xi, 0) n_b(r, \xi) r dr d\xi d\phi - se \int E_z(r, \xi) n_b(r, \xi) r dr d\xi d\phi \quad (2.63)$$

where  $dV = r dr d\xi d\phi$  [I think].

### 2.3.4 Notes Bonatto

Rate of change due to the longitudinal electric field acting on an electron beam, i.e position beam in the decelerating region of the wakefield.

"the beam only experiences its self-excited wakefield."

In the passive beam dump, are we essentially slowing down a "drive bunch" without having a witness bunch behind to get accelerated?

It is probably better to use gamma as in Bonatto's paper, to make it easier to explain total beam energy integral. Basically integrate over all particles.

$$U = \gamma m_e c^2 - \frac{dU}{ds} = (F_e)_z = eE_z \quad (2.64)$$

where  $s$  is the distance travelled in the plasma and  $U$  is the energy of a particle in the beam at position  $\xi$ . for ultra relativistic beams,  $\beta \sim 1$ , the longitudinal electric field is a function of the position along the bunch  $\xi = z - ct$  and not  $z$  explicitly.

$$U(s, \xi) = U_0 - esE_z(\xi) \quad (2.65)$$

The total energy of the beam after travelling a distance  $s$  is then found by integrating across all the particles in the beam, which is integrating across  $\xi$  since analysis is in 1-D.

$$U(s) = U_0 \int_{-\infty}^{\infty} \quad (2.66)$$

We will proceed by calculating the gamma factor of a given particle in the beam who's energy we wish to compute.

$$\gamma(s, \xi) = \gamma_0 - esE_z(\xi) \quad (2.67)$$

# 3

## Simulations

- Ways to simulate plasmas, different techniques/codes etc.

### 3.1 Plasma simulations

#### Why simulations

Simulations because: Cheaper than experiments, more readily available to anyone, simulations allow us to study, understand and exploit these phenomena without the need to repeatedly perform expensive and intricate experiments...Furthermore, by having a simulated rather than physical experiment, one may avoid the uncertainties and noise present in the real world and may therefore investigate and even discover physical phenomena that are too sensitive to be detected in noisy data samples. To take advantage of simulations it is however crucial to know the accuracy by which the simulations model the physical situation and to understand the limitations that this imposes. For instance, as will be shown in section XXX, failing to model the experiment with high enough resolution can lead to phenomena emerging from purely numerical features in the simulations. One must therefore be confident that the results seen in simulations accurately represent the physics at hand, either by comparing the simulations to experimental data or theoretical calculations if available. The non-linear nature of the high-energy plasma wakefield phenomena that we wish to model in this project do not lend themselves easily to analytical treatments. To investigate these phenomena and provide useful results for future experiments we will make extensive use of simulations in this project.

Given that a plasma is no more than electrons and ions interacting electromagnetically, the response of such a plasma to the propagation of an electron bunch or laser pulse could in theory be simulated by solving Maxwell's equations for a set of initial conditions. This would involve solving Maxwell's equations at time an initial time  $t_0$  and calculating the combined electromagnetic fields acting on each particle in the plasma. Then, by considering each particles velocity, one could calculate the new positions and velocities of all particles for a small time increase  $t_0 + \Delta t$ . Repeating these computation would lead us to find the approximate plasma response at any arbitrary time  $t > t_0$ . However, this approach is computationally intractable. Since if we attempt this approach in most plasma simulations. For instance, if we consider that the plasma in a typical plasma wakefield accelerator [Hanahoe] is on the order of centimetres in extent, with a number density  $10^{20} m^{-3}$ , we find that we have on the order of  $10^{14}$  electrons in the plasma. All these electrons would have to be included in the simulation and stored with their associated 6-dimensional position and velocity data  $(x, y, z, v_x, v_y, v_z)$ . Each number would be stored as a 32-bit double precision floating point number, yielding the total data size required for the whole plasma simulation on the order

of a petabyte ( $10^{15}$  bytes).

To circumvent this computational road block we make use of so-called Particle-In-Cell (PIC) codes, in which a large collections of physical microscopic particles are represented as smaller collections of macroscopic pseudo-particles on a grid. In this chapter we outline the general PIC approach and introduce the plasma physics PIC code EPOCH, which is used throughout this project. We further detail the modifications necessary to allow the hybrid beam dump scheme to be simulated on EPOCH.

## 3.2 Particle-in-Cell Codes

Starting from EM fields  $\mathbf{E}_{(n)}$ ,  $\mathbf{B}_{(n)}$  and charge current  $\mathbf{J}_{(n)}$  present at iteration  $n$  [at a specific position, middle of Yee grid?] we obtained the fields at the next time step  $n+1$  by computing the resulting fields and currents at an intermediate half-way step  $n + 1/2$ . We do this by first computing the change in the electric field, using Ampere's law,  $\Delta\mathbf{E}_{(n)}$  which we add to our current field such that

$$\mathbf{E}_{(n+1/2)} = \mathbf{E}_{(n)} + \frac{\Delta t}{2} \left( c^2 \nabla \times \mathbf{B}_{(n)} - \frac{\mathbf{J}_{(n)}}{\epsilon_0} \right) \quad (3.1)$$

from this the magnetic field is given by

$$\mathbf{B}_{(n+1/2)} = \mathbf{B}_{(n)} - \frac{\Delta t}{2} \left( c^2 \nabla \times \mathbf{E}_{(n+1/2)} \right) \quad (3.2)$$

(at which point the particle pusher, detailed below, updates the current to  $\mathbf{J}_{(n+1)}$ )  
at which point we need to update the current to  $\mathbf{J}_{(n+1)}$  in order to proceed finding the fields at time step  $n + 1$ . This is done using the particle pusher. We update the position of each particle

$$\mathbf{x}_{(n+1/2)} = \mathbf{x}_{(n)} + \frac{\Delta t}{2} \mathbf{v}_{(n)} \quad (3.3)$$

from which we also obtain the intermediate velocity  $\mathbf{v}_{(n)}$  [correct?]. Using the Lorentz force law we then compute the force  $\mathbf{F}_{(n)} = \Delta p / \Delta t$  which gives the momentum at  $n + 1$  as

$$\mathbf{p}_{(n+1)} = \mathbf{p}_{(n)} + q \Delta t \left[ \mathbf{E}_{(n+1/2)} (\mathbf{x}_{(n+1/2)}) + \mathbf{x}_{(n+1/2)} \times \mathbf{B}_{(n+1/2)} (\mathbf{x}_{(n+1/2)}) \right] \quad (3.4)$$

where, the electric fields are extrapolated (?) to the intermediate point  $n + 1/2$ . Then, using  $\mathbf{p} = \gamma m \mathbf{v}$ , we can find the velocity at  $n + 1$ , from which we then have the current  $\mathbf{J}_{(n+1)}$ . We then reverse the order of computing such that the magnetic field is calculated prior to the electric field,

$$\mathbf{B}_{(n+1)} = \mathbf{B}_{(n+1/2)} - \frac{\Delta t}{2} \left( c^2 \nabla \times \mathbf{E}_{(n+1/2)} \right) \quad (3.5)$$

$$\mathbf{E}_{(n+1)} = \mathbf{E}_{(n+1/2)} + \frac{\Delta t}{2} \left( c^2 \nabla \times \mathbf{B}_{(n+1)} - \frac{\mathbf{J}_{(n+1)}}{\epsilon_0} \right) \quad (3.6)$$

Using these fields when then calculate the new particles positions  $\mathbf{x}_{(n)}$ , we "push" the particles, thus completing the iteration step.

### 3.3 EPOCH

The Extensible PIC Open Collaboration project (EPOCH) is an advance relativistic electromagnetic PIC code developed at the University of Warwick by XXX et al. [ref.user-manual]. EPOCH is now maintained and developed through the Collaborative Computational Project in Plasma Physics (CCP-Plasma), from which access to the code is granted to non-profit research laboratories and Universities [CCP website]. Simulations using EPOCH simply require users to specify the parameters and initial conditions of the simulations without the need to interact with the underlying PIC code. This code is written in Fortran and allows for simulations to be run on multiple parallel processors via MPI, enabling large 1D, 2D or 3D simulations to be run on remote computing clusters. The core PIC in EPOCH is based upon the field update and particle push algorithm of the Plasma Simulation Code (PSC) written by H. Ruhl []. This approach follows closely the algorithms of the SRC code [ref]. [compare with fig3.1 hanahoe thesis]

#### 3.3.1 Input deck and initial conditions

#### 3.3.2 Grid settings

An important feature of PIC codes is the grid parameters. When setting up the resolution of the grid one has to make sure that the grid is sufficiently fine such that the smallest features of our physical system are resolved. This is to ensure that the simulation accurately models the physical system it is meant to represent, to the extent that missing small scale phenomena might alter the large scale outcome of the simulation. A finer grid however requires more macroparticles to fully populate the grid, which inevitably extends the computational time. In addition the time step  $\Delta t$  needs to be suitably decreased as well. This is because of the so-called Courant-Friedrichs-Lowy (CFL) condition. Any simulation introduces uncertainties in the final outcome due to the finite resolution. We need to make sure that the uncertainties introduced during each iteration do not build up and grow unbounded.

Parameters and initial conditions are defined using an *input.deck* file.

```
begin:boundaries
  bc_x_min = simple_laser
  bc_x_max = simple_outflow
  bc_y_min = simple_outflow
  bc_y_max = simple_outflow
end:boundaries

$$n_b = \frac{1}{\sigma_x \sigma_y^2 (2\pi)^{3/2}} e^{-(x-x_0)^2/2\sigma_x^2} e^{-(y-y_0)^2/2\sigma_y^2} e^{-(z-z_0)^2/2\sigma_z^2}$$

```

### 3.3.3 Non-analytical bunch initialisation

- Issue: restart not possible with laser.
- EPOCH allows for a user to manually override particle-parameter distributions defined in the input deck, in which all functions must be defined analytically. By overriding this so-called autoloader, which takes the analytical distributions in the input deck and distributes the macro particles accordingly, this manual approach allows for the initialisation of a bunch with non-analytical density and momentum distributions.
- Furthermore, even if the density distribution were to be easily described analytically, this method offers the advantage that it also overrides the maxwellian velocity distribution that epoch assigns to each bunch of particles in the input deck. This is fine for an initial bunch in thermal equilibrium, but as soon as plasma interaction occurs the velocity distribution of the electrons in the bunch is noticeably non-maxwellian
- VisIt - export data from .sdf file, convert to -csv, read with ic module when compiling epoch.
- (show below, it is possible to have a laser appear before the bunch at some time t, but the parameters of this laser could not be changed so testing several differnt laser intensities, distances etc. would take far too long if the bunhc was forced to propagate 20cm each time before the laser was ramped up )

```

ExportDBAtts = ExportDBAttributes()
ExportDBAtts.allTimes = 0
ExportDBAtts.dirname = "/Users/oscarjakobsson/Documents/epoch-4.14.4/epoch2d"
ExportDBAtts.filename = "test"
ExportDBAtts.timeStateFormat = "%04d"
ExportDBAtts.db_type = "Xmdv"
ExportDBAtts.db_type_fullname = "Xmdv_1.0"
ExportDBAtts.variables = ("Particles/Ek/edriver", "Particles/Weight/edriver")
ExportDBAtts.writeUsingGroups = 0
ExportDBAtts.groupSize = 48
ExportDBAtts.opts.types = (0)
ExportDBAtts.opts.help = ""
ExportDatabase(ExportDBAtts)
ExportDBAtts = ExportDBAttributes()
ExportDBAtts.allTimes = 0
ExportDBAtts.dirname = "/Users/oscarjakobsson/Documents/epoch-4.14.4/epoch2d"
ExportDBAtts.filename = "test"
ExportDBAtts.timeStateFormat = "%04d"
ExportDBAtts.db_type = "Xmdv"
ExportDBAtts.db_type_fullname = "Xmdv_1.0"
ExportDBAtts.variables = ("Particles/Ek/edriver", "Particles/Weight/edriver")
ExportDBAtts.writeUsingGroups = 0
ExportDBAtts.groupSize = 48
ExportDBAtts.opts.types = (0)
ExportDBAtts.opts.help = ""
ExportDatabase(ExportDBAtts)

```

## 3.4 Notes.

Meeting Guoxing:

- We will change  $\sigma_{x,y}$ , in simulation from  $\sigma_{x,y} = 0.3\mu m \rightarrow 5 - 10\mu m$  because the  $0.3\mu m$  EuPRAXIA beam parameter gives to high beam density  $n_b$ , which means that we can't have  $n_b \sim n_p$  because the plasma density would have to be too high. We should aim for  $n_p \sim 10^{17} - 10^{18} \sim n_b$  (standard L/PWFA) parameters. EuPRAXIA wants  $\sigma_{x,y}$  small because small bunches gives more coherent radiation in undulators. One could expand the beam by letting it propagate freely (expand due to space charge) a distance before reaching the beam dump.

- Run simulations with uniform plasma density for  $n_p$ :

$n_p \sim 0.1n_b$	Non-linear
$n_p \sim n_b$	Quasi-linear
$n_p \sim 10n_b$	Linear
- Use  $\Delta E/E = 0.01$  and bunch charge 30 pC (5 fs).
- Estimate necessary simulation propagation length by saturation length using wave-

### 3. Simulations

---

breaking electric field gradient

$$L_{\text{sat}} \approx \frac{T_0}{eE_{\text{wb}}} = \frac{T_0}{e} \frac{e}{m_e c \omega_p} = \frac{T_0}{m_e c} \sqrt{\frac{m_e e \epsilon_0}{e^2 n_b}}$$

- Project outline:
  - Uniform plasma with varying  $n_b \sim n_p$
  - Vary plasma density profile
  - Test laser to dump head of beam
  - Run simulations for real FlashForward parameters and not the idealized Eu-PRAXIA parameters.

- 100pC

$$n_b = \frac{N_p}{(2\pi)^{3/2} \sigma_y^2 \sigma_x} = \frac{6.25 \times 10^8}{(2\pi)^{3/2} (5 \times 10^{-6})^3} \approx 3.2 \times 10^{23} \text{ m}^{-3}$$

$$\Rightarrow eE_{\text{wb}} = \begin{cases} 17 \text{ GeV/m} & n_p = 0.1 n_b \\ 54 \text{ GeV/m} & n_p = n_b \\ 172 \text{ GeV/m} & n_p = 10 n_b \end{cases} \Rightarrow L_{\text{sat}}(1 \text{ GeV}) = \begin{cases} 5.8 \text{ cm} & n_p = 0.1 n_b \\ 1.9 \text{ cm} & n_p = n_b \\ 0.6 \text{ cm} & n_p = 10 n_b \end{cases}$$

$$1 \text{ GeV beam} \Rightarrow L_{\text{sat}} \sim 2 \text{ cm} = 2 * 10^4 \mu\text{m}$$

- 30pC

$$n_b = \frac{N_p}{(2\pi)^{3/2} \sigma_y^2 \sigma_x} = \frac{1.87 \times 10^8}{(2\pi)^{3/2} (5 \times 10^{-6})^3} \approx 9.5 \times 10^{22} \text{ m}^{-3}$$

$$\Rightarrow eE_{\text{wb}} = \begin{cases} 9.4 \text{ GeV/m} & n_p = 0.1 n_b \\ 30 \text{ GeV/m} & n_p = n_b \\ 94 \text{ GeV/m} & n_p = 10 n_b \end{cases} \Rightarrow L_{\text{sat}}(1 \text{ GeV}) = \begin{cases} 10.7 \text{ cm} & n_p = 0.1 n_b \\ 3.4 \text{ cm} & n_p = n_b \\ 1.1 \text{ cm} & n_p = 10 n_b \end{cases}$$

$$1 \text{ GeV beam} \Rightarrow L_{\text{sat}} \sim 3.4 \text{ cm} = 3.4 * 10^4 \mu\text{m}$$

# 4

## Simulation tests

### 4.1 Plasma deceleration - Uniform density

#### 4.1.1 Transverse instabilities in quasilinear regime

### 4.2 Hybrid Scheme - Feasibility study

#### 4.2.1 Initialising a decelerated bunch

- Compare to actual already propagated bunch we want to simulate. See how quickly the uniform plasma resembles that of the plasma of the propagated simulation. If it takes long time then the laser results might not represent the real situation. Compare simulations side by side as both real and initialised bunches propagate further, see if any deviations occur or if the bunch I set up is actually a fair approximation (compare energy, particle number etc.)

#### 4.2.2 Introduction of co-propagating laser

- Results with respect to laser intensity/amplitude/wavelength as well as distance from bunch.

#### 4. Simulation tests

---

# 5

## Ongoing and future work

Having constructed the necessary computational framework for simulating the hybrid beam dump scheme we can now investigate the feasibility of this scheme and proceed to work out the details of the bunch-laser interaction. This will include investigating and optimizing the distance at which the laser is introduced, the spatial separation between the bunch and the laser, the intensity and pulse length of the laser and effects caused by the difference in phase velocity between the bunch and the laser.

Once the details of the hybrid scheme has been investigated and a desirable approach has been determined we should proceed by high resolution simulations to verify that that the scheme works. As we have seen in section XXX the effect of insufficiently high simulation resolution can yield wildly different outcomes, as small effects can become amplified or neglected, in comparison to higher resolution runs. Consequently, in order to obtain reliable results from our simulations it is crucial to investigate the parameters that determine the resolution of the simulation. These include:

- The number of grid points: where a finer grid will increase the spatial resolution by having the macro-particles in adjacent grid cells be closer together, thus allowing the distribution of the plasma and bunch electrons to be more accurately modelled. This however comes at the cost of longer computational time.
- The number of macro particles in each grid cell: this has the same effect as using a finer grid by allowing the contents of grid cells to more accurately describe the distribution of micro-particles in those cells, since if only one macroparticle was used in a cell with electrons of varying energy and momentum that macroparticle would have to average these properties and thus remove the finer details of the plasma and bunch.
- The number of macro particles in the electron bunch: This number is crucial to accurately capture the small-scale effects on the bunch caused by the interaction with the plasma electrons.

How to establish these simulation parameters?

## 5. Ongoing and future work

---

We may divide the work on the hybrid scheme into three broad areas.

- Energy loss w.r.t bunch and plasma parameters
  - Eloss(bean width)
  - Eloss(length)
  - Eloss( $n_p/n_b$ ), where  $n_p = n_p(\text{beam width, beam length})$
- Simulation parameters
  - Grid settings and resolution to avoid transverse instabilities
  - Minimise numerical noise using laser ramp
  - Accuracy vs. Computational cost
- Laser driver
  - Optimise laser parameters
    - \* Time when introduced in simulation (at/before saturation)
    - \* Distance from bunch
    - \* Pulse length
    - \* Intensity, wavelength
    - \* Laser ramp
  - Further laser investigations
    - \* Multiple consecutive laser pulses

# 6

## Conclusion

Lorem ipsum dolor sit amet, consectetur adipisicing elit, sed do eiusmod tempor incididunt ut labore et dolore magna aliqua. Ut enim ad minim veniam, quis nostrud exercitation ullamco laboris nisi ut aliquip ex ea commodo consequat. Duis aute irure dolor in reprehenderit in voluptate velit esse cillum dolore eu fugiat nulla pariatur. Excepteur sint occaecat cupidatat non proident, sunt in culpa qui officia deserunt mollit anim id est laborum.

## 6. Conclusion

---

# Bibliography

- [1] John David Jackson. Jackson - Classical Electrodynamics (3rd Ed.).pdf, 1962.
- [2] John M Dawson. Electron Oscillations in a Cold Plasma. Technical Report 2, 1959.
- [3] W. Lu, C. Huang, M. Zhou, M. Tzoufras, F. S. Tsung, W. B. Mori, and T. Katsouleas. A nonlinear theory for multidimensional relativistic plasma wave wakefields. *Physics of Plasmas*, 13(5), 2006.
- [4] A. Bonatto, C. B. Schroeder, J. L. Vay, C. R. Geddes, C. Benedetti, E. Esarey, and W. P. Leemans. Compact disposal of high-energy electron beams using passive or laser-driven plasma decelerating stage. *AIP Conference Proceedings*, 1777(1):0–5, 2016.

## Bibliography

---

# A

## Appendix: Input decks